Plinabulin, an inhibitor of tubulin polymerization, targets KRAS signaling through disruption of endosomal recycling

Cimino, Patrick J ; Huang, Lan ; Du, Lihua ; Wu, Yanping ; Bishop, Jamie ; Dalsing-Hernandez, Jessica ; Kotlarczyk, Kari ; Gonzales, Paul ; Carew, Jennifer ; Nawrocki, Steffan ; Jordan, Mary Ann ; Wilson, Leslie ; Lloyd, G Kenneth ; Wirsching, Hans-Georg

Abstract: Constitutive activation of Kirsten rat sarcoma viral oncogene homolog (KRAS) is the most common oncogenic event in certain types of human cancer and is associated with poor patient survival. Small molecule signaling inhibitors have improved the clinical outcomes of patients with various cancer types but attempts to target KRAS have been unsuccessful. Plinabulin represents a novel class of agents that inhibit tubulin polymerization with a favorable safety profile in clinical trials. In the present study, the potency of plinabulin to inhibit tubulin polymerization and growth of KRAS-driven cancer cells was characterized. efficacy of plinabulin was tested in two different mouse models; one being the RCAS/t-va gene transfer system and the other being a xenograft model. cell culture tubulin polymerization assays were used to complement the mouse models. There was improved survival in a KRAS-driven mouse gene transfer glioma model, but lack of benefit in a similar model, without constitutively active KRAS, which supports the notion of a KRAS-specific effect. This survival benefit was mediated, at least in part, by the ability of plinabulin to inhibit tubulin polymerization and disrupt endosomal recycling. It was proposed a mechanism of compromised endosomal recycling of displaced KRAS through targeting microtubules that yields inhibition of protein kinase B, but not extracellular signal regulated kinase (ERK) signaling, therefore lending rationale to combination treatments of tubulin- and ERK-targeting agents in KRAS-driven cancer.

DOI: https://doi.org/10.3892/br.2019.1196

Title: **Plinabulin, an inhibitor of tubulin polymerization, targets KRAS signaling through disruption of endosomal recycling**

Authors: Patrick J. Cimino,[1] Lan Huang,[2] Lihua Du,[2] Yanping Wu,[2] Jamie Bishop,[3] Jessica Dalsing-Hernandez,[4] Kari Kotlarczyk,[4] Paul Gonzales,[4] Jennifer S. Carew,[5] Steffan T. Nawrocki,[5] Mary Ann Jordan,[3] Leslie Wilson,[3] George K. Lloyd,[2] Hans-Georg Wirsching,[6]

Affiliations:
[1] Department of Pathology, University of Washington, Seattle, WA
[2] BeyondSpring Pharmaceuticals Inc., New York City, NY
[3] Biomolecular Science and Engring, University of California, Santa Barbara, CA
[4] Translational Drug Development Inc., Scottsdale, AZ
[5] Institute for Drug Development, University of Texas, San Antonio, TX ; Present Address: University of Arizona, Tucson, AZ.
[6] Department of Neurology, University Hospital Zurich, Zurich, CH.

Corresponding Author:
Hans-Georg Wirsching, MD
Department of Neurology
University Hospital Zurich
Frauenklinikstr. 26
CH-8091 Zurich
Switzerland
Phone: +41-44-255-5500
Email: hans-georg.wirsching@usz.ch

Running title: Tubulin inhibition targets KRAS signaling

Keywords: Plinabulin; KRAS; Endosome; Tubulin; Cancer

ABSTRACT

Constitutive activation of KRAS is the most common oncogenic event in human cancers and is associated with poor patient survival. Small molecule signaling inhibitors have improved the clinical outcomes of patients with various cancer types, but attempts to target KRAS have been unsuccessful. Plinabulin represents a novel class of agents that inhibit tubulin polymerization with a favorable safety profile in clinical trials. Here, we characterize the potency of plinabulin to inhibit tubulin polymerization and growth of KRAS-driven cancer cells. *In vivo* efficacy of plinabulin was tested in two different mouse models; one being the RCAS/t-va gene transfer system and the other being a xenograft model. Cell culture including tubulin polymerization assays. In vitro cell culture tubulin polymerization assays were used to complement the mouse models. There was improved survival in a KRAS-driven mouse gene transfer glioma model, but lack of benefit in a similar model without constitutively active KRAS, supports the notion of a KRAS-specific effect. This survival benefit was mediated, at least in part, by the ability of plinabulin to inhibit tubulin polymerization and disrupt endosomal recycling. We propose a mechanism of compromised endosomal recycling of displaced KRAS through targeting microtubules that yields inhibition of Akt, but not ERK signaling, thus lending rationale to combination treatments of tubulin- and ERK-targeting agents in KRAS-driven cancers.

INTRODUCTION

Activating point mutations in Kirsten Rat Sarcoma Viral Oncogene Homolog (KRAS) are present in approximately 30% of human cancers, including the vast majority of pancreatic cancers and large fractions of lung, colon and breast cancers (1). Moreover, elevation of the activity of KRAS and other ras family members due to upstream signaling is very common throughout most types of cancer (2). KRAS is a small GTP-ase that mediates survival, proliferation and cytoskeletal organization of cancer cells by transducing or enhancing down-stream signals of the MEK/extracellular signaling-regulated kinase (ERK) and of the phosphoinositide 3-kinase (PI3K)/Akt signaling cascade (3). Presence of constitutively active KRAS is associated with chemotherapy resistance and poor patient outcome, but thus far attempts to directly target KRAS have failed (4). KRAS exerts its functions at the inner cellular membrane and requires continuous recycling of mislocalized protein through endosomes. The microtubule network is critically involved in this subcellular segregation and trafficking of endosomal recycling (5, 6). Drugs that target microtubules include taxanes and *vinca alcaloids*. These drugs are among the best studied, longest standing cancer drugs and act as microtubule stabilizers that slow or block mitosis at the metaphase–anaphase transition, eventually yielding apoptosis (7). Tissue penetration of taxanes and *vinca alcaloids* is however limited and the therapeutic index is low.

Plinabulin (NPI-2358) is a synthetic analogue of halimide, an *Aspergillus*-derived natural product that targets the tubulin network through a mechanism that is distinct from that of taxanes and *vinca* alcaloids: instead of stabilization of polymerized microtubules,

plinabulin inhibits polymerization by interacting with the colchicine-binding domain of β-tubulin (8, 9). Drugs that target the colchicine-binding domain were historically deemed too toxic to be effective anti-cancer agents, but novel compounds such as plinabulin are more specific and potent inhibitors of tubulin polymerization (7), and tissue penetration is more favorable compared to classic tubulin stabilizing drugs (10). Moreover, plinabulin showed a favorable safety profile and encouraging antitumor responses in two early phase clinical trials (10, 11). Based on these results, plinabulin is currently in phase III clinical development in combination with docetaxel, and in phase I/II in combination with nivolumab for advanced non-small cell lung cancer (NCT02504489, NCT02812667). Here we detail the inhibition of tubulin polymerization by plinabulin, report preclinical results of the efficacy of plinabulin in KRAS driven murine tumor models and outline effects of plinabulin on intracellular KRAS trafficking and down-stream signaling.

MATERIALS AND METHODS

Compounds and Reagents

Plinabulin was obtained from BeyondSpring Pharmaceuticals, Inc. (New York, NY), irinotecan was obtained from Teva Pharmaceuticals (Irvine, CA), docetaxel and paclitaxel were from Selleckchem (Houston, TX). For *in vivo* studies, all compounds were diluted in 5% dextrose for intraperitoneal (i. p.) or intravenous (i. v.) injection of indicated doses. For *in vitro* studies, all drugs were diluted in complete growth media with 1 % dimethyl-sulfoxide (DMSO).

Tubulin polymerization assays

MTP preparations consisting of 70% tubulin and 30% microtubule-associated proteins (MAPs) were isolated from bovine brain, polymerized into microtubules and monitored by light scattering at 350 nm. Transmission electron microscopy was used to determine the mean length distribution of microtubules in the absence or presence of drug. Grids were viewed in a Jeol electron microscope-1200 EX11 at 2000X and 30,000X magnification. The Zeiss MOPIII was used to determine microtubule length distributions and mean lengths for at least 100 microtubules per sample.

Cell culture

All cell lines were obtained from the American Type Culture Collection (ATCC, Manassas, VA). HCT-15, A549, and MDA-MB-231 cells were maintained in RPMI-1640 medium (Lonza, Walkersville, MD). LoVo cells were maintained in F12-K medium (Corning/Cellgro, Manassas, VA). DF1 cells were maintained in Dulbecco's Modified Eagle's medium (DMEM). All cell culture media were supplemented with 10% fetal bovine serum (FBS; Seradigm, Radnor, PA) and housed in a 5% CO2 atmosphere at 37°C, except DF1 cells were cultured at 39°C.

Immunocytology

A549 cells were seeded overnight on coverslips. Cells were fixed in 4% paraformaldehyde for 10 minutes, followed by permaeabilization utilizing 0.1% Triton in PBS for 5 minutes and blocking of unspecific binding with 5% donkey serum in PBS. These steps were done at room temperature, and washing with PBS was done between

any steps. Primary antibodies were rabbit anti-early endosomal antigen (EEA)1 (1:300, Thermo Scientific, Waltham, MA) and mouse anti-KRAS (1:100, Thermo Scientific), and were applied overnight at 4°C. After additional washing steps, cells were incubated with secondary donkey anti-rabbit-488 (1:200) and anti-mouse-Cy3 (1:200) antibodies in PBS with 5% donkey serum for 30 minutes at roomtemperature, followed by washing and addition of Hoechst 33342 Solution (1 µg/ml, Thermo Scientific) for 3 min, followed by washing, H_2O for 3 min, 100% ethanol for 3 min and air-drying prior to embedding. Images were taken with a Zeiss LSM 780 NLO confocal microscope and quantification was done utilizing Image J (NIH, Bethesda, MD).

In Vitro Cell Viability Assays

Indicated cell lines were grown in standard serum-containing media. Cell viability was measured in triplicate utilizing the adenosine triphosphate (ATP)-based CellTiter-Glo® assay (Promega, Madison, WI).

Murine xenograft models

Animal studies were carried out in accordance with the Guide for the Care and Use of Laboratory Animals, as adopted by the U.S. National Institutes of Health. Animal research was prospectively approved by the Institutional Animal Care and Use Committee (Animal assurance institutional #A3226-01; Protocol #50842). Female athymic Foxn1nu mice between 4 to 6 weeks of age were obtained from Harlan (Madison, WI). For the HCT-15 and LoVo models, mice were anesthetized by isoflurane and inoculated with 0.1 ml of a 50% media / 50% matrigel mixture containing a

suspension of cultured tumor cells (1 x 10^7 cells/mouse for LoVo, 5 x 10^6 cells/mouse for HCT-15). As the tumors grew, the length (largest diameter) and width (smallest diameter) of tumors were measured using a digital caliper to determine the mean radius for tumor volume estimates assuming a spherical geometry and calculation per $V_{tumor} = 4/3 \times \pi \times r^3$. Automated calculation and documentation of tumor volume estimates was done using the animal study management software Study Director V.2.1.1 (Studylog Systems, San Francisco, CA). When tumor volume estimates exceeded ~~a predetermined size~~ 50-60 mm^3, mice were randomized into control and treatment groups, being pair-matched by tumor size, and dosing was initiated (Day 1).

RCAS/t-va glioma models

N/t-va;Ink4a/$Arf^{-/-}$ mice expressing the avian t-va receptor under control of the nestin promoter were injected intracranially with DF-1 cells as hosts for the replicative avian retroviral gene transfer vector RCAS. Tumors were generated utilizing two RCAS vectors for the expression of platelet-derived growth factor B (PDGFB), and either KRAS encoding the activating mutation $KRAS^{G12A}$, or green fluorescent protein (GFP). DF-1 cells infected with these RCAS strains were injected into the brains of adult mice (aged 4 to 6 weeks) under the anesthetic isoflurane. One microliter of a 1:1 mixture for a total combined injection of 4 x 10^4 transfected DF-1 cell suspension was delivered using a 30-gauge needle attached to a Hamilton syringe. Coordinates were bregma 0 mm, lateral -0.5 mm (right of midline), and depth -1.5 mm from the dural surface. Mice were put on the study when they lost > 0.3 grams total over 2 consecutive days or displayed outward signs of a tumor. The mice were euthanized in a carbon dioxide chamber when

they lost more than 20% of their body weight, displayed a lack of mobility, inability to feed or weighed less than 14 grams for a male/ 12 grams for a female. Groups were treated with vehicle or plinabulin at 7.5 mg/kg twice per week for up to 10 weeks.

RESULTS

Plinabulin inhibits microtubule polymerization

The overlapping binding sites of plinabulin and colchicine at the α/β-tubulin interface led us to first characterize and compare effects of both drugs on microtubule dynamics. In a cell-free MTP-containing model system, plinabulin inhibited microtubule formation more potently than colchicine, as measured by turbidity spectra (Figure 1A). The concentrations of plinabulin and colchicine at which polymerization was inhibited 50% (IC_{50}) were 2.4 µM (standard deviation [SD] +/- 0.4, N=4 independent experiments) and 7.6 µM (SD +/- 2.4, N=3), respectively. The tubulin polymerization profiles obtained in the presence of different concentrations of plinabulin or colchicine differed in two ways: First, the initial rate of increase in absorbance over time decreased with increasing drug concentrations of plinabulin, indicating that there is a lag period for microtubule formation. In contrast, the initial rate of polymerization is unchanged at all concentrations of colchicine. Second, microtubule formation in the presence of plinabulin does not reach steady state at high drug concentrations, as indicated by the absorbance values that increase linearly with time, whereas in the presence of high concentrations of colchicine steady state is readily reached. These data are suggestive of a reduction of the pool of soluble, assembly-competent tubulin in the presence of plinabulin. In contrast, colchicine binds nearly irreversibly and induces a rate-limiting

conformational change in tubulin that, once incorporated into the lattice, inhibits further microtubule polymerization at substoichiometric concentrations (12). Transmission electron microscopy was performed to further validate these findings. No microtubule aggregates were identified in the presence of plinabulin 1.25 µM (Figure 1B) and 2.5 µM (data not shown). The mean microtubule length was however potently reduced to 34% of DMSO-treatment at 1.25 µM plinabulin, whereas colchicine 1.25 µM reduced the mean microtubule length to 63% (Figure 1C, Supplementary Figure 1). Next, we evaluated how these findings translated in a cellular system. The IC_{50} of plinabulin for inhibiting mitosis in MCF-7 breast cancer cells was 17 nM and mitosis was halted at the prometaphase (Supplementary Figure 2), suggesting that tubulin bound by plinabulin may not be assembly competent to be incorporated into microtubules.

Plinabulin synergizes with chemotherapy in KRAS-driven xenograft cancer models

In consideration of the limited activity of chemotherapy in various cancer types with constitutive KRAS activity, we sought to evaluate whether the distinct mechanism of action of plinabulin yielded anti-tumor activity in these cancers. In a panel of 8 human cell lines derived from pancreatic, colorectal and renal cancers, plinabulin inhibited growth in the nanomolar range in all cell lines, except for the pancreatic cancer cell line HPAC (Figure 2A). This led us to also explore putative anti-cancer effects of plinabulin *in vivo* in a panel of five *KRAS* mutated xenograft models. Contrasting *in vitro* results, plinabulin monotherapy failed to inhibit the growth of LoVo and HCT-15 colorectal cancer (Figure 2B, Supplementary Figure 3A) and exerted no more than a moderate

effect on the growth of MDA-MB-231 breast cancer alone (Figure 2C). The growth of the KRAS mutated DU-145 prostate cancer (Figure 2D) and A549 lung adenocarcinoma (Supplementary Figure 3B) models was neither affected by plinabulin monotreatment. However, in combination with standard chemotherapeutic agents administered in these cancers, we observed additive or synergistic effects of plinabulin on the inhibition of tumor growth, including combinations with the topoisomerase inhibitor irinotecan and with the tubulin targeting agents, paclitaxel and docetaxel (Figure 2, Supplementary Figure 3). These data point towards ~~a modulation of anti-apoptotic signaling pathways rather than direct cytotoxic~~ effects of plinabulin other than direct cytotoxicity and therefore led us to next evaluate down-stream KRAS signaling.

Tubulin depolymerization yields displacement of KRAS to endosomes

In non-small cell lung and other cancers, downstream effects of KRAS signaling include the activation of the MEK/ERK and PI3K/Akt pathways (3). Moreover, ERK is regulated by a variety of converging pathways that are activated under cellular stress including chemotherapy with tubulin-targeting agents, whereas the key activator of Akt is the KRAS target phosphoinositide 3-kinase (PI3K) (13). The proto-oncogene phosphatase and tensin homolog (PTEN) is in reverse the key inhibitor of PI3K, thus rendering intact PTEN a pre-requisite for KRAS-dependency of cancer cells (14). In PTEN proficient A549 lung cancer cells, disassembly of the microtubule network utilizing plinabulin concentrations in the range of its IC_{50} for *in vitro* tubulin depolymerization led to rapid accumulation of KRAS in early endosomes (mean endosomal EEA1-colocalized KRAS in DMSO vs Plinabulin = 2 vs 31 %, $p<0.001$, N=5, Figure 3A). Moreover, overall KRAS

levels were decreased upon plinabulin treatment, which may reflect lysosomal degradation. The two key down-stream effectors of KRAS signaling, ERK and Akt, were differently affected by plinabulin treatment and subsequent KRAS depletion: ERK phosphorylation was increased, but Ser473-phosphorylation of Akt was reduced (Figure 3B). These findings indicate that displacement of KRAS and potentially other tubulin-dependent kinases may yield decreased downstream PI3K signaling, while alternative signaling pathways act on the ERK signaling cascade.

Plinabulin prolongs survival in a RAS-driven glioma model

Next, we aimed to evaluate the specificity of plinabulin effects on KRAS driven cancers in a simplified model system that was not biased by co-mutations. For this purpose we employed two PTEN-proficient glioma gene transfer models that differed solely in the absence or presence of constitutively active KRAS. Gliomas were generated in the brains of Ink4a/Arf-deficient mice expressing the avian t-va receptor under control of the nestin promoter (N/t-va:Ink4a/Arf$^{-/-}$) to allow gene transfer utilizing the avian retrovirus RCAS for overexpression of PDGFB and GFP or KRAS^{G12A}. Although activating KRAS mutations are rare in gliomas, hyperactivation of RAS signaling is a key component of gliomagenesis and histologically, these gliomas resemble the human disease (15). Moreover, given that brain metastases are an important cause of cancer-related death (16-18), we aimed to evaluate whether plinabulin was capable of penetrating the blood brain barrier to a relevant extent. Penetration of the blood-brain barrier by plinabulin is supported by the observation that in a Quantitative Hole Body Autoradioluminogrphy study, plinabulin rapidly entered into the brain parenchyma (Supplemental Figure 4).

Treatment with plinabulin prolonged survival in KRAS-expressing gliomas (Figure 3C), but not in tumors that were solely driven by PDGFB and Ink4a/Arf loss (Figure 3D), thus confirming penetration of the blood brain barrier to a relevant extent and supporting the notion of efficacy of plinabulin specifically in KRAS-mutated tumors.

DISCUSSION

KRAS-driven cancers pose a major therapeutic challenge. To date, precision medicine approaches have failed to directly target KRAS (4), and standard chemotherapy has only limited efficacy in KRAS-mutated cancers (19). KRAS exerts its oncogenic function primarily by activating the MEK/ERK and PI3K/Akt signaling cascades, but dual inhibition of both pathways is deemed too toxic to be clinically applicable. However, targeting microtubules has been suggested as a means to compromise endosomal recycling of KRAS (20) and combination of docetaxel with the MEK-inhibitor selumetinib dramatically improved the survival of patients with KRAS-driven non-small cell lung cancer compared to docetaxel alone in an exploratory, randomized phase II trial (21).

Our preclinical study supports the concept of combining tubulin-targeting agents with inhibitors of the MEK/ERK signaling axis: upon plinabulin treatment, we observed rapid accumulation of KRAS in endosomal vesicles and a potent inhibitory effect on Akt phosphorylation, but a simultaneous increase in ERK activation that may compensate for Akt inhibition. The underlying mechanism of this ERK activation likely reflects a stress response through alternative kinases such as the stress-activated protein kinases (22).

Compensatory ERK activation may also explain the lack of growth inhibition of most xenograft models tested here by plinabulin monotherapy. Moreover, effective targeting of KRAS signaling through combined treatment with tubulin-targeting agents and MEK/ERK inhibitors may require intact PTEN, as disinhibition of PI3K signaling upon loss of PTEN activity renders Akt signaling independent of KRAS.

Plinabulin may be well suited for such potentially toxic combination treatments, given its favorable safety profile and tolerability in clinical trials. Of note, tubulin polymerization assays reported here indicate that plinabulin exerts its effects by a mechanism that is distinct and potentially less toxic than that of colchicine and established anti-cancer tubulin-targeting drugs: plinabulin binds less avidly to tubulin and its binding may be more readily reversible. Moreover, activity in a mutant KRAS-driven brain tumor model underscores the favorable pharmacokinetics profile of plinabulin, including crossing of the blood brain barrier.

In summary, our preclinical study supports the inclusion of tubulin-targeting agents in future developments of combination treatments against KRAS-driven cancers.

Compliance with Ethical Standards:

Funding: This study was funded by BeyondSpring Pharmaceuticals Inc.

Conflict of Interest: LH, LD, YW, and GKL are employed by BeyondSpring Pharmaceuticals Inc. JDH, KK, and PG are employed by Translational Drug Development Inc.

Ethical approval: All applicable international, national, and/or institutional guidelines for the care and use of animals were followed. This article does not contain any studies with human participants performed by any of the authors.

REFERENCES

1. Prior IA, Lewis PD and Mattos C: A comprehensive survey of Ras mutations in cancer. Cancer Res 72: 2457-2467, 2012.

2. Fernandez-Medarde A and Santos E: Ras in cancer and developmental diseases. Genes Cancer 2: 344-358, 2011.

3. Downward J: Targeting RAS signalling pathways in cancer therapy. Nat Rev Cancer 3: 11-22, 2003.

4. Ostrem JM and Shokat KM: Direct small-molecule inhibitors of KRAS: from structural insights to mechanism-based design. Nat Rev Drug Discov 15: 771-785, 2016.

5. Schmick M, Vartak N, Papke B, et al.: KRas localizes to the plasma membrane by spatial cycles of solubilization, trapping and vesicular transport. Cell 157: 459-471, 2014.

6. Thissen JA, Gross JM, Subramanian K, Meyer T and Casey PJ: Prenylation-dependent association of Ki-Ras with microtubules. Evidence for a role in subcellular trafficking. J Biol Chem 272: 30362-30370, 1997.

7. Dumontet C and Jordan MA: Microtubule-binding agents: a dynamic field of cancer therapeutics. Nat Rev Drug Discov 9: 790-803, 2010.

8. Wang Y, Zhang H, Gigant B, et al.: Structures of a diverse set of colchicine binding site inhibitors in complex with tubulin provide a rationale for drug discovery. FEBS J 283: 102-111, 2016.

9. Prota AE, Danel F, Bachmann F, et al.: The novel microtubule-destabilizing drug BAL27862 binds to the colchicine site of tubulin with distinct effects on microtubule organization. J Mol Biol 426: 1848-1860, 2014.

10. Mita MM, Spear MA, Yee LK, et al.: Phase 1 first-in-human trial of the vascular disrupting agent plinabulin(NPI-2358) in patients with solid tumors or lymphomas. Clin Cancer Res 16: 5892-5899, 2010.

11. Millward M, Mainwaring P, Mita A, et al.: Phase 1 study of the novel vascular disrupting agent plinabulin (NPI-2358) and docetaxel. Invest New Drugs 30: 1065-1073, 2012.

12. Ravelli RB, Gigant B, Curmi PA, et al.: Insight into tubulin regulation from a complex with colchicine and a stathmin-like domain. Nature 428: 198-202, 2004.

13. McCubrey JA, Steelman LS, Chappell WH, et al.: Roles of the Raf/MEK/ERK pathway in cell growth, malignant transformation and drug resistance. Biochim Biophys Acta 1773: 1263-1284, 2007.

14. Singh A, Greninger P, Rhodes D, et al.: A gene expression signature associated with "K-Ras addiction" reveals regulators of EMT and tumor cell survival. Cancer Cell 15: 489-500, 2009.

15. Uhrbom L, Dai C, Celestino JC, Rosenblum MK, Fuller GN and Holland EC: Ink4a-Arf loss cooperates with KRas activation in astrocytes and neural progenitors to generate glioblastomas of various morphologies depending on activated Akt. Cancer Res 62: 5551-5558, 2002.

16. Langer CJ and Mehta MP: Current management of brain metastases, with a focus on systemic options. J Clin Oncol 23: 6207-6219, 2005.

17. Khuntia D, Brown P, Li J and Mehta MP: Whole-brain radiotherapy in the management of brain metastasis. J Clin Oncol 24: 1295-1304, 2006.

18. Chaffer CL and Weinberg RA: A perspective on cancer cell metastasis. Science 331: 1559-1564, 2011.

19. Von Hoff DD, Ervin T, Arena FP, et al.: Increased survival in pancreatic cancer with nab-paclitaxel plus gemcitabine. N Engl J Med 369: 1691-1703, 2013.

20. Basseville A, Bates S and Fojo T: Pancreatic cancer: Targeting KRAS and the vitamin D receptor via microtubules. Nat Rev Clin Oncol 12: 442-444, 2015.

21. Janne PA, Shaw AT, Pereira JR, et al.: Selumetinib plus docetaxel for KRAS-mutant advanced non-small-cell lung cancer: a randomised, multicentre, placebo-controlled, phase 2 study. Lancet Oncol 14: 38-47, 2013.

22. Sanchez I, Hughes RT, Mayer BJ, et al.: Role of SAPK/ERK kinase-1 in the stress-activated pathway regulating transcription factor c-Jun. Nature 372: 794-798, 1994.

FIGURE LEGENDS

Figure 1. Plinabulin inhibits tubulin polymerization. **A,** turbidity spectra of cell-free microtubule protein polymerization in the presence of dimethyl sulfoxide (DMSO) drug vehicle, or indicated concentrations of plinabulin (*upper panel*) or colchicine (*lower panel*). **B,** microtubules were allowed to polymerize in the presence of DMSO or 1.25 μM plinabulin for 60 minutes prior to electron microscopy. **C,** frequency histograms of mean microtubule lengths at steady state in the presence of DMSO or plinabulin 2.5 μM.

Figure 2. Plinabulin inhibits tumor growth in *KRAS* mutated cancer models. **A,** *in vitro* growth inhibition of *KRAS* mutated cancer cell lines by plinabulin. 1.000 cells per well were seeded in 96-well plates in triplicate overnight and treated in serum-free medium with plinabulin at $\log_2$ increments of 1 nM-16.4 μM plinabulin in 0.2% DMSO or DMSO 0.2% alone for 72 h prior to assessment of adenosine triphosphate content. **C-D,** human *KRAS* mutated LoVo colon cancer (B), MDA-MB-231 breast cancer (C) and DU-145 prostate cancer (D) xenograft models were injected as indicated with 5% dextrose solution (vehicle) i.p. or i.v., plinabulin (plin) 7.5 mg/kg i.p. on 5 subsequent days, irinotecan 80 mg/kg i.p. once weekly for 3 weeks (B), paclitaxel 16 mg/kg i.p. on 5 subsequent days (C), and docetaxel 12.5 mg/kg i.v. on days 1, 3 and 5 (D). Tumor volumes were measured twice weekly in N=10 mice per treatment group. Linear regression was performed to determine differences in tumor growth over time. n.s., not significant, * $p<0.05$, ** $p<0.01$, *** $p<0.001$, **** $p<0.0001$.

Figure 3. Plinabulin yields endosomal accumulation of KRAS. **A,** A549 cells were treated with 0.2% DMSO (upper panel) or 1.25 μM plinabulin (lower panel) for 2 hours prior to immunofluorescence stainings of DNA utilizing 4,6-Diamidino-2-phenylindole (DAPI, blue), the early endosomal antigen EEA-1 (green) and KRAS (red). Scale bar, 10 μm. **B,** immunoblot analysis of A549 cells serum-starved overnight and treated with 1% DMSO or 1.25 μM plinabulin for 2 hours prior to treatment with 100 ng/ml epithelial growth factor (EGF) for indicated times. **C, D,** Mouse gliomas were generated in N/t-

va;Ink4a/Arf$^{-/-}$ mice by transduction with RCAS-PDGF and RCAS-KRAS^{G12A} (C), or RCAS-GFP (D). Mice were treated with 5% dextrose solution i.p. (vehicle) or plinabulin 7.5 mg/kg i.p. for 5 subsequent days. Weight loss was utilized as a surrogate for tumor formation to determine the timepoint of treatment initialization. Survival was defined as the time from treatment until sacrifice. The log rank test was applied to determine survival difference between groups.

Figure 1

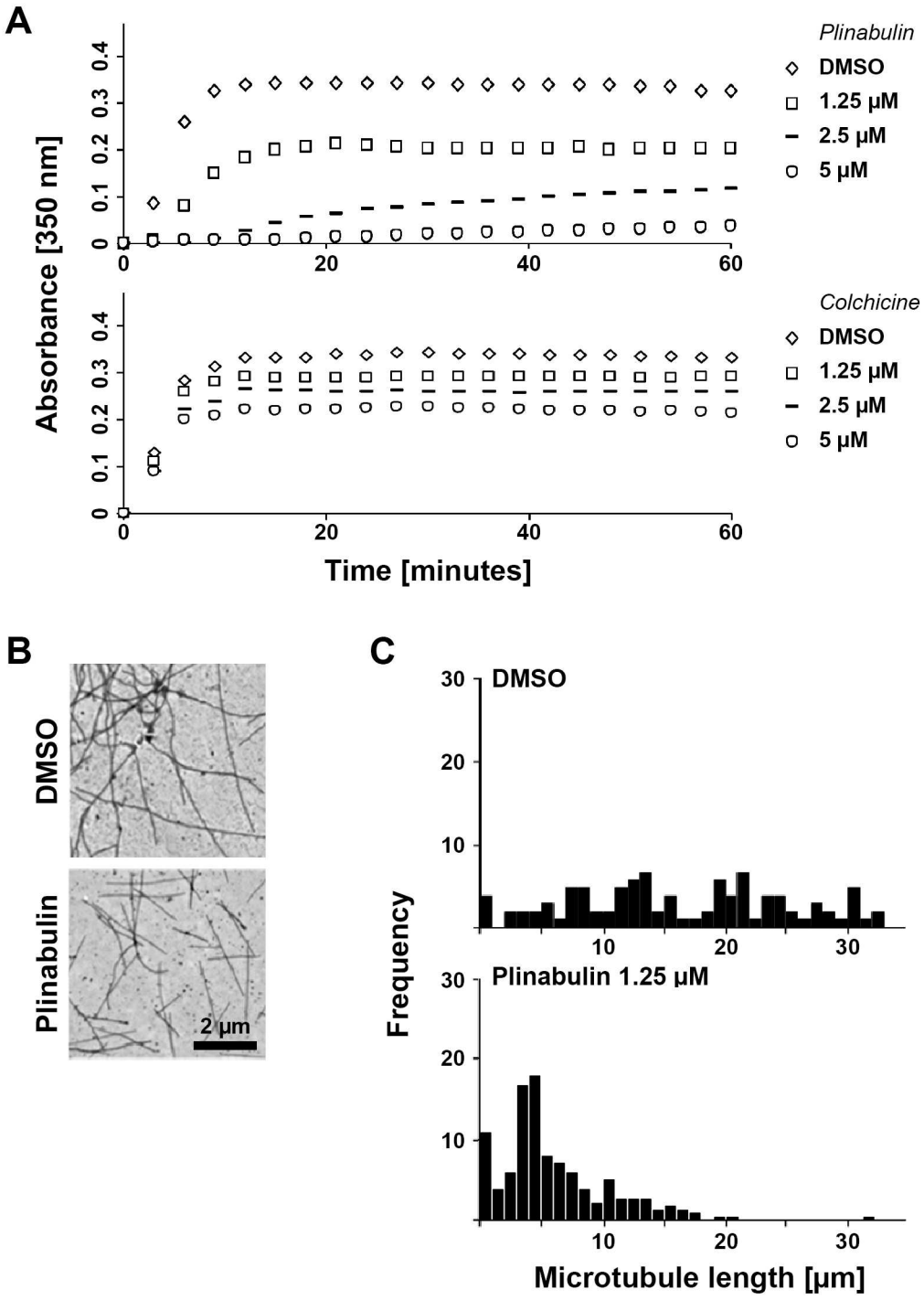
A
Absorbance [350 nm]
0
0.1
0.2
0.3
0.4
0
20
40
60
Time [minutes]
Plinabulin
DMSO
1.25 µM
2.5 µM
5 µM
Colchicine
DMSO
1.25 µM
2.5 µM
5 µM
B
DMSO
Plinabulin
2 µm
C
DMSO
Plinabulin 1.25 µM
Frequency
10
20
30
Microtubule length [µm]

Figure 2

A

Cell line	Cancer type	KRAS mutation	*in vitro* IC_{50} of plinabulin (nM)
HCT-15	colorectal	G13D	13
HCT-116	colorectal	G13D	33
LoVo	colorectal	G13D	7
MDA-MB-231	breast	G13D	14
RXF-393	renal	D153V	4
AsPC-1	pancreatic	G12D	17
Capan-2	pancreatic	G12V	10
HPAC	pancreatic	G12D	>1,000
MIA PaCa-2	pancreatic	G12C	92

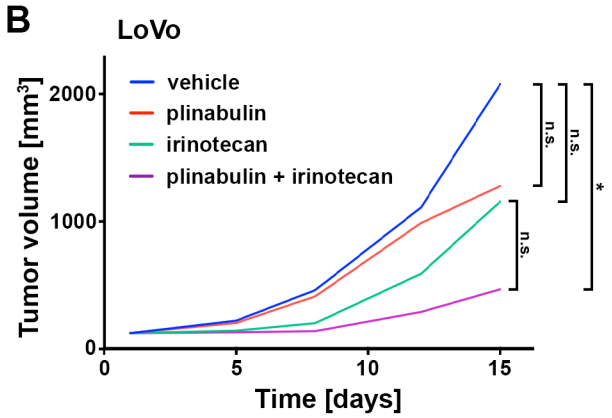

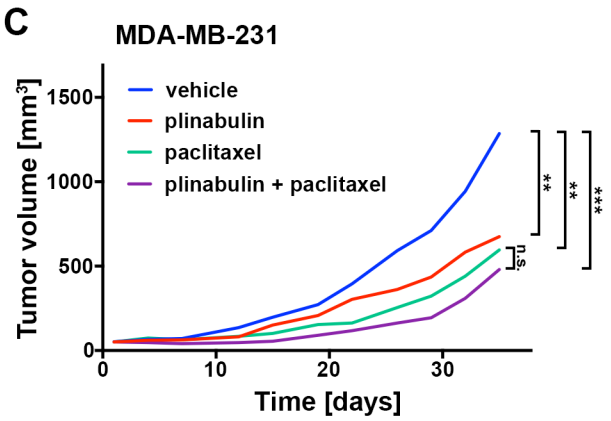

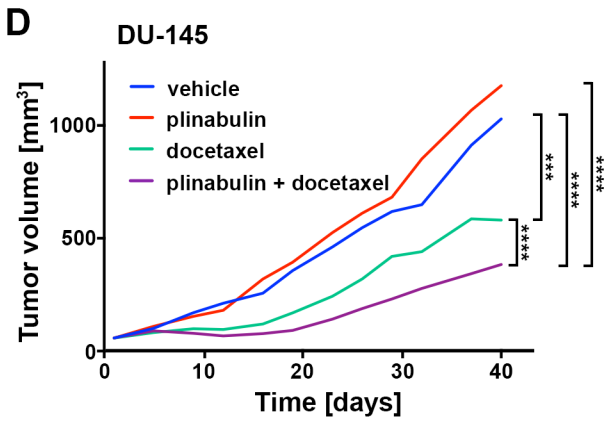

Figure 3

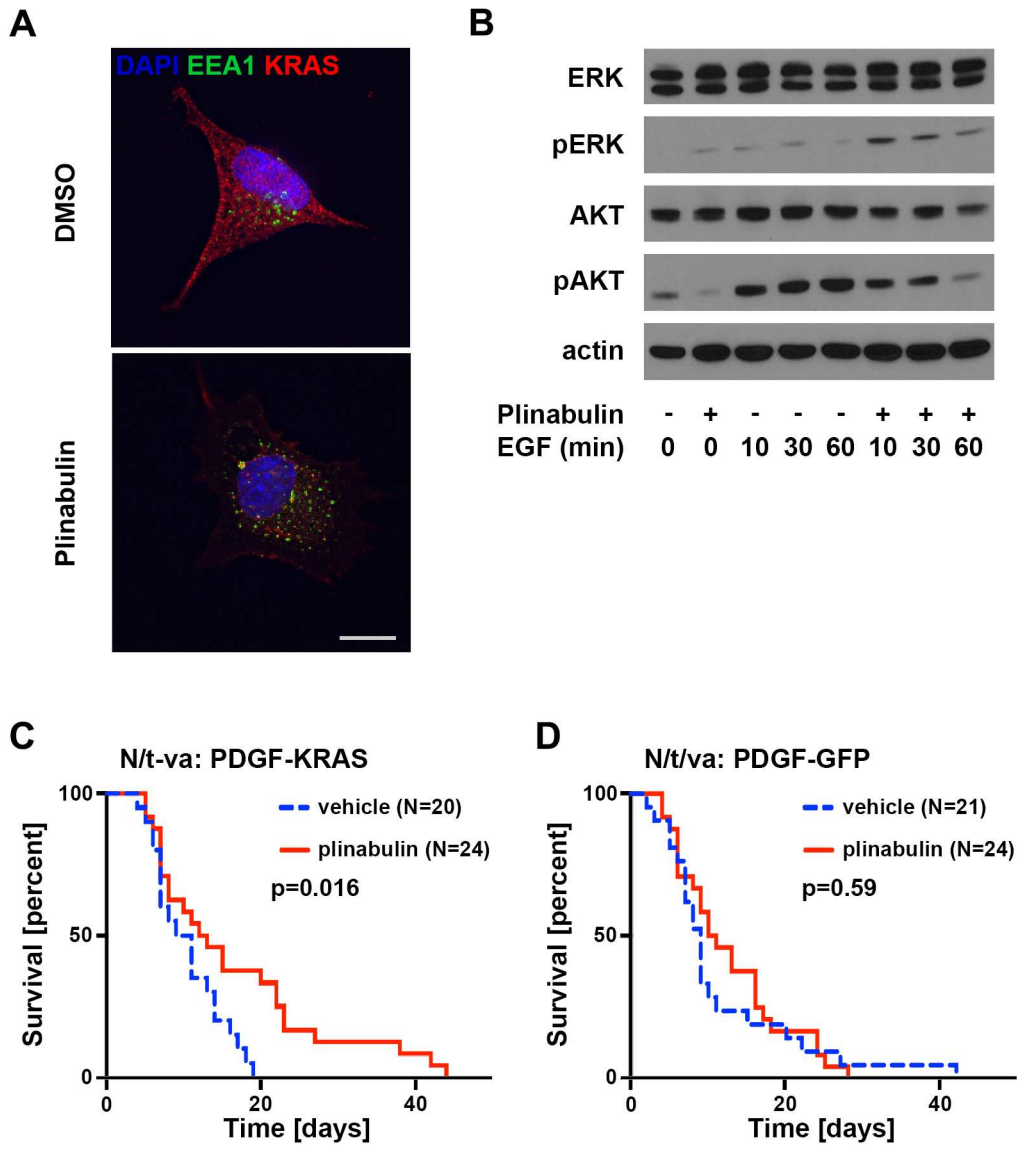
A
DAPI EEA1 KRAS
DMSO
Plinabulin
B
ERK
pERK
AKT
pAKT
actin
Plinabulin - + - - - + + +
EGF (min) 0 0 10 30 60 10 30 60
C
N/t-va: PDGF-KRAS
vehicle (N=20)
plinabulin (N=24)
p=0.016
Survival [percent]
Time [days]
D
N/t/va: PDGF-GFP
vehicle (N=21)
plinabulin (N=24)
p=0.59
Survival [percent]
Time [days]

Supplementary Figure 1

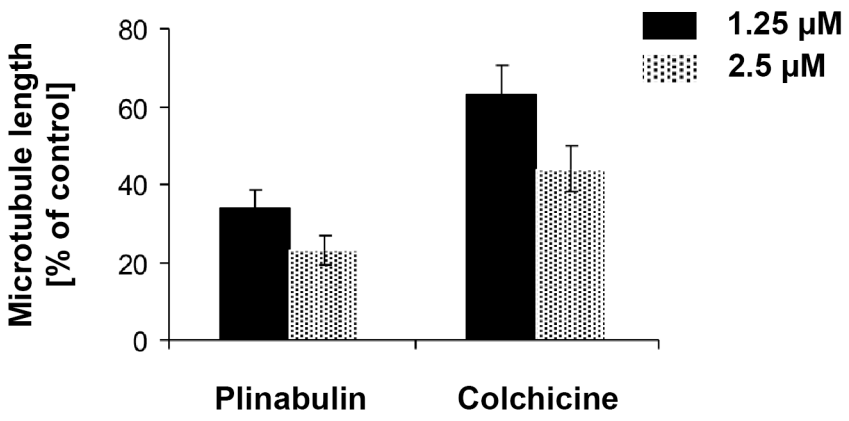

Supplementary Figure 2

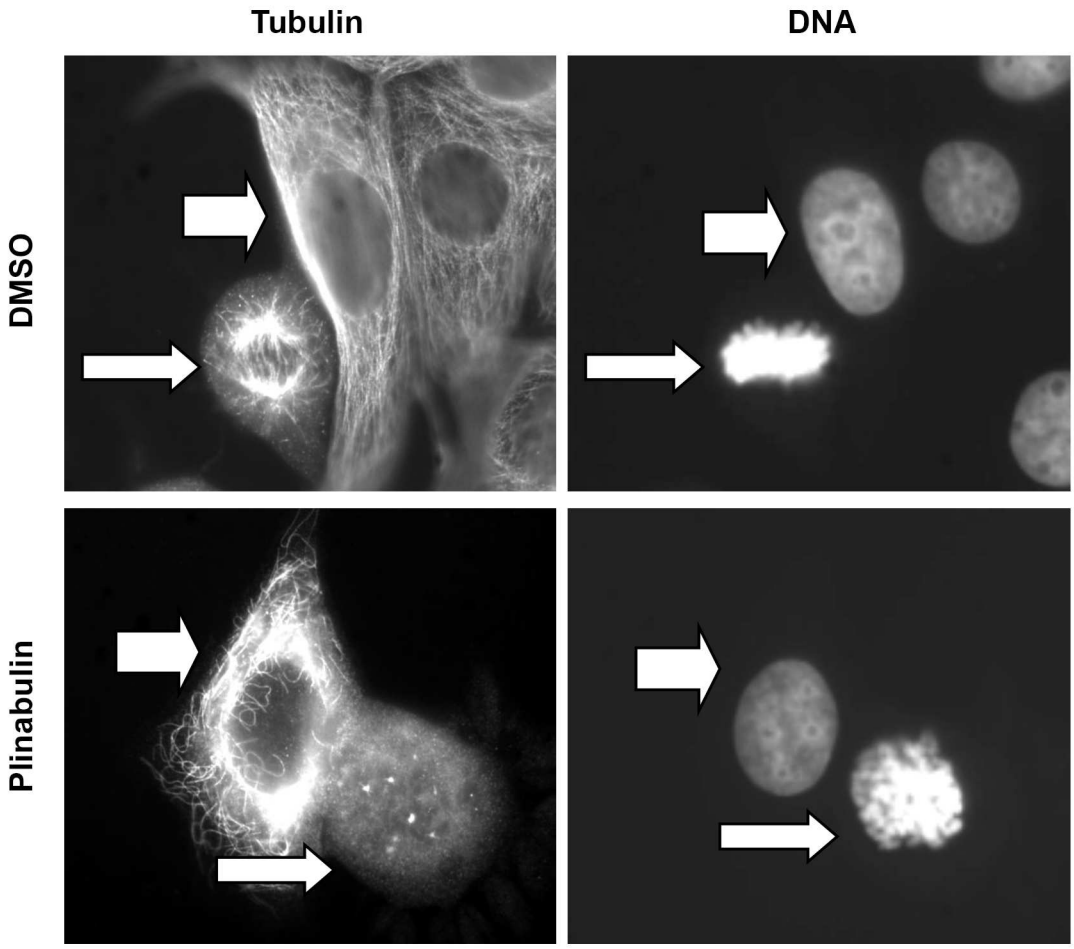

Supplementary Figure 3

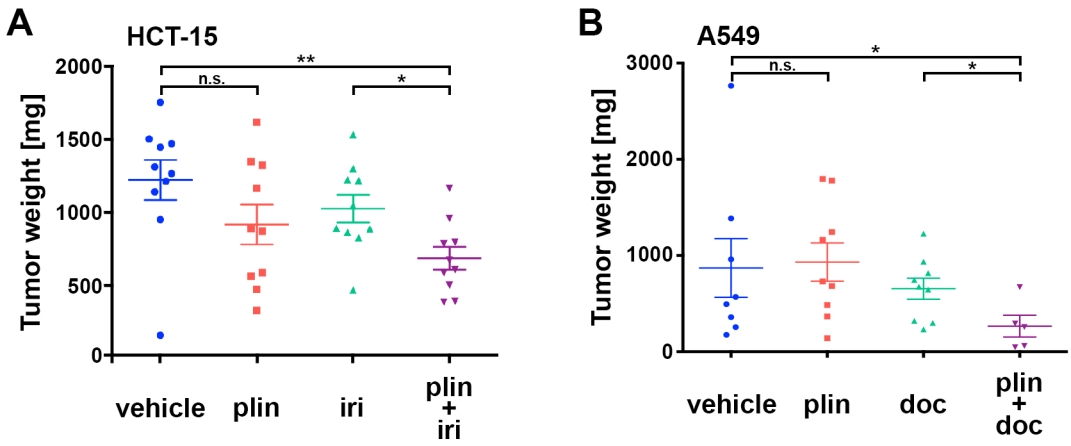

Supplementary Figure 4